Applied Catalysis B: Environmental 165 (2015) 232–244

Contents lists available at ScienceDirect

Applied Catalysis B: Environmental

journal homepage: www.elsevier.com/locate/apcatb

NO_x storage and reduction properties of model manganese-based lean NO_x trap catalysts

Zhao-shun Zhang[a,b], Bing-bing Chen[a,b], Xin-kui Wang[a,b], Li Xu[a,b], Chaktong Au[c], Chuan Shi[a,b,*], Mark Crocker[d,**]

[a] Key Laboratory of Industrial Energy and Environmental Engineering (MOE), Dalian University of Technology, Dalian, China
[b] Laboratory of Plasma Physical Chemistry, Dalian University of Technology, Dalian, China
[c] Chemistry Department, Hong Kong Baptist University, Hong Kong, China
[d] Center for Applied Energy Research, University of Kentucky, Lexington, KY 40511, USA

ARTICLE INFO

Article history:
Received 24 June 2014
Received in revised form
28 September 2014
Accepted 2 October 2014
Available online 13 October 2014

Keywords:
Manganese
Palladium
NO oxidation
NO_x storage-reduction
NO_x adsorber

ABSTRACT

In order to study the role of manganese in LNT catalysis, model Pd/Mn/Ba/Al, Pd/Mn/Al and Pd/Ba/Al catalysts were prepared and characterized. Both Mn-containing catalysts exhibited higher activity for NO oxidation to NO_2 than the Pd/Ba/Al reference catalyst, although NO_x-TPD experiments showed that adsorbed NO_x species were weakly bound on Pd/Mn/Al. Consequently, the presence of Ba was essential for high storage capacity. Compared to the Pd/Ba/Al reference, Pd/Mn/Ba/Al showed significantly improved NO_x conversion under lean-rich cycling conditions as a consequence of its increased activity for NO oxidation and hence, superior NO_x storage efficiency. In addition, the presence of Mn greatly lessened the inhibiting effects of H_2O and CO_2 on cycle-averaged NO_x conversion, this being due to the facile decomposition of manganese carbonate at low temperatures as evidenced by DRIFTS. Significantly, the Pd/Mn/Ba/Al catalyst displayed comparable activity to a traditional LNT catalyst of the Pt/Ba/Al type, showing the promising prospect of such new type of LNT catalysts.

1. Introduction

Vehicular engines operating under lean burn conditions are becoming increasingly popular due to their superior fuel economy as compared to conventional Otto gasoline engines. However, the toxic NO_x exhaust gas components of lean-burn engines cannot be efficiently removed with three-way catalysts, which are effective only under stoichiometric conditions. Consequently, selective catalytic reduction (SCR) of NO_x using urea as a reductant has been developed for mobile lean NO_x removal [1]. While this technology is well suited for heavy duty diesel applications, for light duty applications lean NO_x trap (LNT) catalysts (otherwise known as NO_x storage-reduction (NSR) catalysts) in some cases to offer a cheaper and more practical alternative [2]. LNT catalysts work under cyclic conditions of fuel-lean and fuel-rich environments. Under lean exhaust conditions, when oxygen is in excess, NO_x is adsorbed on the catalyst; under rich conditions, when an excess of reductants is present, NO_x reduction takes place. In principle, a LNT catalyst should have sites for NO_x sorption (alkali metal or alkaline earth metal compounds) and sites for NO_x oxidation/reduction (noble metals). Platinum and barium deposited on γ-Al_2O_3 (Pt/Ba/Al catalyst) is the most commonly studied model composition for NO_x storage-reduction catalysis [3,4].

Many studies have focused on the use of different catalyst compositions and operating conditions, given that they have a great impact on NO_x storage and reduction performance [5,6]. Vijay et al. found that Co exhibits an ability similar to that of Pt to oxidize NO during the lean phase [7,8], while it is limited by its poor activity for catalyst regeneration during the rich phase. Addition of ceria to Pt/Ba/Al catalysts is reported to improve NO_x storage capacity at low temperatures (<300 °C), while catalyst regeneration behavior is also improved as a consequence of the better dispersion of Pt on CeO_2 compared to BaO [9]. Manganese is also found to be an effective additive for Ba-based LNT catalysts. Le Phuc et al. [10–12] found that Mn addition to Pt/Ba/Al improved NO_x storage capacity and led to an improvement of NO_x reduction (conversion and selectivity to N_2) at 400 °C. Xiao et al. [13] found that Mn/Ba/Al exhibited

* Corresponding author at: Key Laboratory of Industrial Energy and Environmental Engineering (MOE), Dalian University of Technology, Dalian, China. Tel.: +86 411 84986083.
** Corresponding author at: Center for Applied Energy Research, University of Kentucky, Lexington, KY 40511, USA. Tel.: +1 859 257 0295.
E-mail addresses: chuanshi@dlut.edu.cn (C. Shi), mark.crocker@uky.edu (M. Crocker).

http://dx.doi.org/10.1016/j.apcatb.2014.10.001
0926-3373/

good catalytic activity for NO oxidation-storage under lean burn conditions. The beneficial incorporation of Mn in a variety of mixed oxides intended for NO_x storage applications has also been reported [14–19], while Li et al. [20] have demonstrated that when incorporated in a LNT catalyst, Mn-containing perovskites can exhibit NO oxidation activity similar to that of Pt-based catalysts. However, to date most studies concerning the NO_x storage-reduction performance of Mn-containing catalysts have not been performed in the presence of CO_2 and H_2O. In this context, it should be noted that manganese (II) carbonate decomposes at low temperatures (<200 °C) [21]; hence, it might be expected that carbon dioxide would not exert a significant inhibition effect on the catalytic properties of Mn in LNT catalysts.

In the present study, model Pd/Mn/Ba/Al LNT catalysts were prepared for comparison with LNT catalysts of the Pd/Ba/Al and Pd/Mn/Al type, in order to study the role of manganese in LNT catalysis. Pd was selected as the precious metal owing to its low cost in comparison with Pt and Rh, which provides a strong incentive for its use in commercial applications. However, while Pd is reasonably active for NO_x reduction, it is possesses poor activity for NO oxidation [22,23]. However, if Pd can be augmented by a base metal such as Mn, which is active in NO oxidation, then the opportunity might exist to decrease or even eliminate the use of Pt in LNT catalysts. Specific goals of this study were to clarify the effects of Mn addition on (i) the microstructure of the LNT catalysts, (ii) NO oxidation and storage capacity, and (iii) the catalytic properties under NO_x storage-reduction cycling. In order to compare the inhibiting effects of H_2O and CO_2 on the Pd/Ba/Al and Mn-containing catalysts, experiments were conducted in both the presence and absence of H_2O and CO_2.

2. Experimental

2.1. Catalyst preparation

Catalyst samples were prepared by incipient wetness impregnation. In the case of Pd/Ba/Al (hereafter denoted by the sample code PBA), γ-Al_2O_3 was impregnated with an aqueous solution of $Ba(O_2CCH_3)_2$, dried and calcined at 500 °C for 5 h in air. The Ba-loaded γ-Al_2O_3 was subsequently impregnated with aqueous palladium nitrate ($Pd(NO_3)_2{\cdot}2H_2O$ dissolved in 0.1 mol/l nitric acid), dried and further calcined at 500 °C for 5 h. Pd/Mn/Ba/Al (PMBA) was prepared by the following method: the γ-Al_2O_3 support was impregnated with aqueous $Ba(O_2CCH_3)_2$, followed by drying and calcination at 500 °C in air, after which the product was impregnated with aqueous $Mn(NO_3)_2$, dried and calcined at 500 °C in air. The resulting solid was impregnated with Pd as described above. Pd/Mn/Al (PMA) was similarly prepared but with omission of the $Ba(O_2CCH_3)_2$ impregnation step. The target Pd, Mn and Ba loadings were 1 wt.%, 10 wt.% and 20 wt.%, respectively. The reference catalyst Pt/20Ba/Al_2O_3 (hereafter denoted by the sample code Pt-BA) was prepared by the incipient wetness method according to a literature procedure [24].

2.2. Catalyst characterization

Surface area analysis was performed according to the BET method by nitrogen adsorption at −196 °C using a JW-BK122 W system. Prior to the measurements catalyst samples were outgassed overnight at 160 °C under vacuum. Transmission electron microscopy (TEM) images of the catalysts were obtained on a JEOL JEM-2000 (EX Japan) microscope operated at 120 kV. Powder X-ray diffraction (XRD) measurements were performed on an X-ray diffractometer (Rigaku D-Max Rotaflex) using Cu Kα radiation. Temperature programmed reduction (H_2-TPR) experiments on the as-synthesized catalysts were performed using a Micromeritics AutoChem II Analyzer equipped with a TCD detector to monitor H_2 uptake. Samples (about 50 mg) were heated from room temperature to 600 °C at a rate of 10 °C/min under flowing 5% H_2/Ar (50 ml/min). Prior to TPR, samples were pre-treated in Ar at 120 °C for 1 h to remove adsorbed water. The actual metal content in the catalysts was determined by inductively coupled plasma-atomic emission spectroscopy (ICP-AES, Optima 2000DV). X-ray photoelectron spectroscopic (XPS) measurements were conducted using an Al Kα source operated at 10 kV and 15 mA. Binding energies were corrected for charging effects by referencing them to adventitious carbon (284.6 eV).

2.3. NSC and NOC experiments

NO_x storage capacity (NSC) and NO oxidation capacity (NOC) experiments were performed in a microreactor using a chemiluminescence NO_x analyzer (Ecotech ML9841AS) as the detector. Prior to both sets of measurements, the catalyst (150 mg) was pretreated at 500 °C in flowing 1% H_2/Ar for 1 h. NSC and NOC measurements were then performed by exposing the catalyst to flowing gas containing 500 ppm NO, 8% O_2, with or without 2% H_2O and 2% CO_2 present, and balance N_2, at 200, 300 and 400 °C. The storage time was 50 min for the NSC experiments. NOC was measured when steady state had been achieved, i.e., when the catalyst was completely saturated with NO_x (typically requiring 2–3 h). NSC and NOC experiments were operated at a gas hourly space velocity (GHSV) of 100,000 h^{-1}. The NSC and NOC were calculated according to the following formula:

$$\mathrm{NSC} = \frac{\int_0^{t_s} (\mathrm{NO}_{x,\mathrm{in}} - \mathrm{NO}_{x,\mathrm{out}})dt}{m_{\mathrm{cat}}} \quad (1)$$

where t_s is the storage time (s) and m_{cat} is the mass of the catalyst (g).

$$\mathrm{NOC} = \frac{\mathrm{NO}_{2,\mathrm{out}}}{\mathrm{NO}_{\mathrm{in}}} \times 100\% \quad (2)$$

2.4. NO_x-TPD

The stability of adsorbed NO_x species was evaluated by means of NO_x-TPD measurements using 150 mg of catalyst contained in a microreactor. Each catalyst sample was first pretreated at 500 °C for 60 min in flowing 1% H_2/Ar and then cooled to 200 °C in flowing Ar. NO_x adsorption was carried out for 50 min at 200 °C using feed gas containing 500 ppm NO, 8% O_2 and balance Ar, with or without 2% H_2O and 2% CO_2 present. After flushing the catalyst with Ar at 200 °C for 30 min, the temperature was increased to 700 °C at a rate of 10 °C/min in flowing Ar. Effluent gases were analyzed on-line using a mass spectrometer (Pfeiffer Vacuum GSD 301). All flow conditions were operated at a gas hourly space velocity (GHSV) of 30,000 h^{-1}.

2.5. Catalyst evaluation

Catalyst evaluation was performed in a quartz reactor tube loaded with ca. 150 mg of catalyst particles (20–40 mesh). Effluent gases were analyzed on-line using a mass spectrometer (Pfeiffer Vacuum GSD 301) and a specific FTIR (Sick Maihak S710). All flow conditions were operated at a gas hourly space velocity (GHSV) of 30,000 h^{-1}. Before each experiment the catalyst was pretreated in 1% H_2/Ar flow at 500 °C for 1 h. Following pre-treatment, the catalyst was cooled to the measurement temperature, after which lean-rich cycling was performed until the catalyst reached a cycle-average steady state.

Table 1
Gas composition used for NO_x storage/reduction cycling experiments.

Parameter	Lean	Rich
Duration (s)	120	10
Temperature (°C)	200–400	200–400
Space velocity (h^{-1})	30,000	30,000
NO (ppm)	500	–
O_2 (%)	8	–
H_2 (%)	–	3
H_2O (%)	–/2	–/2
CO_2 (%)	–/2	–/2
Ar (%)	Balance	Balance

The NO_x concentration was averaged over 20 cycles to give a mean conversion according to the following formula:

$$NO_x \text{ conversion} = \frac{\int_0^t (NO_{x,in} - NO_{x,out})dt}{\int_0^t NO_{x,in}dt} \times 100\% \quad (3)$$

The cycling parameters and gas composition used for the cycling experiments are summarized in Table 1. NO, NH_3 and NO_2 by mass spectrometry, N_2O by specific FTIR (Sick Maihak S710). The N_2 selectivity is calculated assuming no other N-compounds than NO, NO_2, N_2O, and NH_3.

2.6. In situ DRIFTS study of NO_x storage

In situ DRIFTS was performed on a Tensor 27 (Bruker) FTIR spectrometer equipped with an in situ diffuse reflection chamber with CaF_2 windows and a high-sensitivity MCT detector. The catalyst for the DRIFTS studies was finely ground and placed in a stainless steel crucible in the sample chamber. Mass flow controllers and a temperature controller were used to simulate the conditions used in the NO_x storage capacity tests. All gas mixtures were fed at a flow rate of 100 ml/min. Prior to recording each DRIFTS spectrum, the catalyst was pretreated in 1% H_2 at 500 °C for 30 min and then cooled to the measurement temperature under flowing Ar in order to acquire a reference spectrum. A gas mixture of 500 ppm NO, 8% O_2 with or without 2% H_2O and 2% CO_2 present, and Ar as the balance was then introduced, and a series of NO_x adsorption spectra were obtained over time. All spectra reported here were collected at a resolution of 4 cm^{-1} for 60 scans.

3. Results and discussion

3.1. Catalyst characterization

The elemental compositions and surface areas of the catalysts were determined by ICP-AES and N_2 physisorption measurements, respectively, the results being collected in Table 2. The BET surface areas of the catalysts decreased slightly with respect to the bare alumina upon manganese and barium incorporation, indicative of some degree of pore filling.

X-ray diffractograms of PBA, PMA and PMBA are shown in Fig. 1. The characteristic reflections of Pd and PdO were not observed due to the low concentration of Pd in the catalysts and/or the small size of the Pd particles. X-ray diffraction (XRD) analysis showed that the main phases present in PMA were γ-Al_2O_3 (JCPDS No. 47-1770) and Mn_2O_3 (JCPDS No. 24-0735), thereby confirming the decomposition of $Mn(NO_3)_2$ into crystalline Mn_2O_3 during catalyst calcination. In addition, the $MnAl_2O_4$ spinel (JCPDS No. 29-0880) is also observed for PMA (as shown in the inset of Fig. 1), indicating that manganese and aluminum oxides reacted to form the spinel during calcination, in accordance with the results of Strohmeier et al. [25]. In the case of PBA and PMBA, the presence of $BaCO_3$ is evident based on data for $BaCO_3$ (JCPDS No. 41-0373) in the ICDD

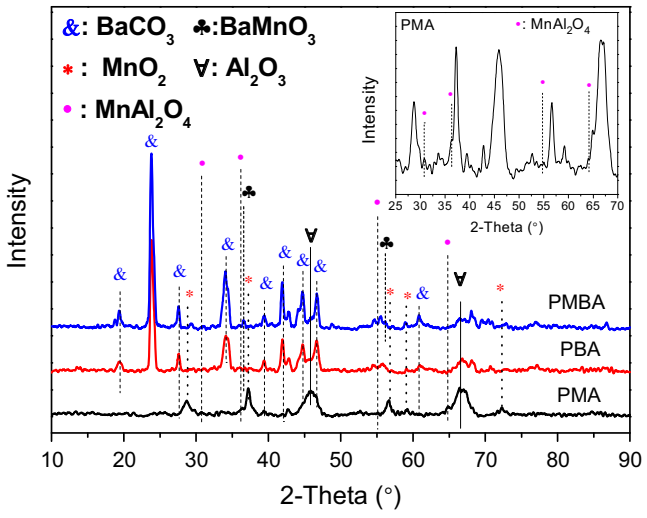

Fig. 1. XRD patterns of PBA, PMA and PMBA catalysts.

PDF Database, consistent with the decomposition of $Ba(O_2CCH_3)_2$ into crystalline $BaCO_3$ during catalyst calcination. There might have two types of $BaCO_3$ species, i.e., monoclinic and witherite. As pointed out by Baiker that the metastable monoclinic phase transformed easily into the thermodynamically stable orthorhombic $BaCO_3$ (witherite) at ambient conditions [26]. Since, all the samples in the present study were aged in air for several days or weeks, thus, the crystalline form of $BaCO_3$ should be witherite for the PBA and PMBA samples. In the case of PMBA, the sample showed diffraction patterns for $BaCO_3$, γ-Al_2O_3 and $BaMnO_3$ (JCPDS No. 26-0168). However, the presence of some crystalline MnO_x cannot be ruled out, given the detection limit for XRD measurements.

The reducibility of PBA, PMA and PMBA was studied by H_2-TPR, the results of which are shown in Fig. 2. For comparison, the H_2-TPR profiles of MnO_x, Mn/Al and Mn/Ba/Al were also recorded (MnO_x preparation procedures were described in the literature [27], Mn/Al and Mn/Ba/Al were similarly prepared as described in Section 2.1, but with omission of the Pd impregnation step).

Fig. 2(a) shows the H_2-TPR profiles recorded over MnO_x, Mn/Ba/Al and Mn/Al, respectively. Over MnO_x, there are two H_2 consumption peaks at ca. 284 and 430 °C, and the ratio of the lower temperature peak to the higher temperature peak was about 2. The lower temperature peak should be attributed to the reduction of MnO_2 to Mn_3O_4, whereas the higher temperature peak should be attributed to the reduction of Mn_3O_4 to MnO [27,28]. For the Mn/Al sample, two peaks of H_2 consumption were observed at 349 and 412 °C, corresponding to the reduction of $MnO_2 \rightarrow Mn_3O_4 \rightarrow MnO$ [29]. Notably, the H_2 consumption peaks shifted to higher temperatures for Mn/Al sample when Mn was supported on γ-Al_2O_3. According to XRD data, the $MnAl_2O_4$ spinel is also observed for PMA (as shown in Fig. 1), and the higher reduction temperature for Mn/Al sample can be attributed to that a strong interaction between Mn and Al. However, the TPR profiles of the Mn/Ba/Al were greatly different from those of the Mn/Al. In the case of Mn/Ba/Al, there are three reduction peaks at 322, 358 and 505 °C. The peaks at 322 and 358 °C are ascribed to the stepwise reduction of MnO_x. It is noticed that the peak at ca. 505 °C could not be observed over MnO_x and Mn/Al samples, it is reasonable to deduce that the peak at 505 °C is due to the reduction of $BaMnO_3$ perovskite (according to XRD data, the $BaMnO_3$ perovskite is also observed for PMBA as shown in Fig. 1), and this result is consistent with the literature [30].

H_2-TPR profiles of the PBA, PMA and PMBA catalysts were performed to investigate the relative reducibility of the catalysts, as

Table 2
Summary of ICP-AES, BET, Pd particle size and dispersion data for as-prepared catalysts.

Catalyst	Pd (wt.%)	Ba (wt.%)	Mn (wt.%)	BET area (m^2/g)	Pd particle size[a] (nm)	Pd dispersion[b] (%)
γ-Al_2O_3	–	–	–	198	–	–
PBA	0.60	12.6	–	142	3.7	30.2%
PMA	0.84	–	5.29	128	5.6	20.0%
PMBA	0.61	10.3	5.92	126	3.9	28.7%

[a] Average value of 200 Pd particles in TEM image.
[b] Deduced from the expression $D_{dispersion} = 112/d$. Assumes spherical particles and a Pd surface atom density of 1.27×10^{19} atoms/m^2 [33].

shown in Fig. 2(b). For the PMA sample, two peaks of H_2 consumption were observed at 123 and 218 °C, the lower temperature peak should be attributed to the reduction of MnO_2 to Mn_3O_4, whereas the higher temperature peak should be attributed to the reduction of Mn_3O_4 to MnO. Obviously, the reduction temperatures shifted to lower regions, and this phenomenon is often interpreted in terms of the activation and spillover of hydrogen from the initially reduced Pd to MnO_x, and facilitated the reduction of the oxides [31,32]. For PMBA sample, there are two reduction peaks are positioned at 142 and 308 °C, respectively. The peak at 308 °C, as evidenced by the reduction profile of Mn/Ba/Al, should be assigned to the reduction of Mn^{4+} to Mn^{2+} in the lattice of $BaMnO_3$. The assignment of the low temperature peak at 142 °C may be attributed to the overlapped reduction of MnO_x [29,30].

Fig. 3 shows TEM images and Pd particle size histograms of the catalysts, while a summary of the mean Pd particle sizes and Pd dispersions in these samples is given in Table 2. In all cases the Pd nanoparticles are dispersed on the support surface, an average of particle size of 3–6 nm being determined from the TEM images (based on measurement of 200 Pd particles) for the PBA and PMBA samples. While some larger Pd particles could be observed over the PMA sample, indicating the poorer dispersion of Pd on MnO_x/Al_2O_3 support [33]. According to TEM micrographs (Fig. 3(a)), the average Pd particle size in the PBA catalyst (3.7 nm) is close to the value determined for PMBA (Fig. 3(c), 3.9 nm), while the PMA catalyst showed a larger average particle size of 5.6 nm (Fig. 3(b)). These values correspond to Pd dispersions of 30.2% and 28.7%, respectively, for PBA and PMBA, the Pd dispersion of PMA being significantly lower (20.0%).

The results of XPS measurements provide further insight into the dispersion of Pd and Ba in the catalysts. As shown in Table 3, although the Pd content in PMA measured by ICP-AES is higher than that in PBA and PMBA (0.84 wt.%, 0.60 wt.% and 0.61 wt.%, respectively, shown in Table 2), the atomic Pd concentration in PMA determined by XPS is obviously lower than that in PBA and PMBA (0.077%, 0.095% and 0.108%, respectively) [34]. This is indicative of the poor Pd dispersion in PMA which is consistent with the TEM results (Table 2 and Fig. 3). This is also reflected in the lower Pd/Al atomic ratio of PMA (0.27) compared to PBA (0.40) and PMBA (0.45). Moreover, the similar Ba/Al ratios of PBA and PMBA samples suggest that the dispersion of Ba on Al_2O_3 is not influenced by Mn addition, i.e., the Mn is mainly dispersed on the surface of the alumina support, and the barium is not covered by manganese. However, the Mn/Al atomic ratio of PMBA is obviously higher than that of PMA (10.14 and 5.06, respectively). As previously observed by XRD (Fig. 1), the $MnAl_2O_4$ spinel is detected for PMA but not for PMBA, suggesting that the addition of Ba decreases the interaction between Mn and Al, and the manganese dispersion has been improved.

Fig. 4 shows the O 1s and Mn 2p XPS spectra of the PBA, PMA and PMBA samples. By deconvoluting the O 1s signals, the distribution of oxygen species was estimated, the results being given in Table 4. There were two kinds of oxygen species, the peak at BE = 530.5–531.4 eV being assigned to surface lattice oxygen (O_{latt}^{2-}) species, while that at BE = 532.0–532.9 eV is assigned to adsorbed oxygen species (O_{ads}) [27,35]. As indicated in Table 4, the ratio of O_{ads}/O_{latt}^{2-} was 0.665 for PMA, higher than that for PBA and PMBA (0.105 and 0.270 respectively), indicating that there is an increase in the concentration of surface oxygen species after Mn addition to PBA. The Mn $2p_{3/2}$ regions of the XPS spectra are shown in Fig. 4(d) and (e). By means of curve-fitting, it is evident that there are two kinds of Mn species present; one, with a Mn 2p binding energy in the range of 641.5–641.7 eV, is assigned to Mn^{3+}, while that in the range 642.8–643.8 eV is ascribed to Mn^{4+} [27]. As indicated in Table 4, the ratio of Mn^{4+}/Mn^{3+} was 0.748 in PMA, higher than that in PMBA (0.496). These results indicate that compared to PMBA, PMA is enriched with surface Mn^{4+} species. This is consistent with the O_{ads}/O_{latt}^{2-} data which show PMA has more surface oxygen than PMBA, which can be attributed to the higher Mn^{4+}/Mn^{3+} ratio of PMA.

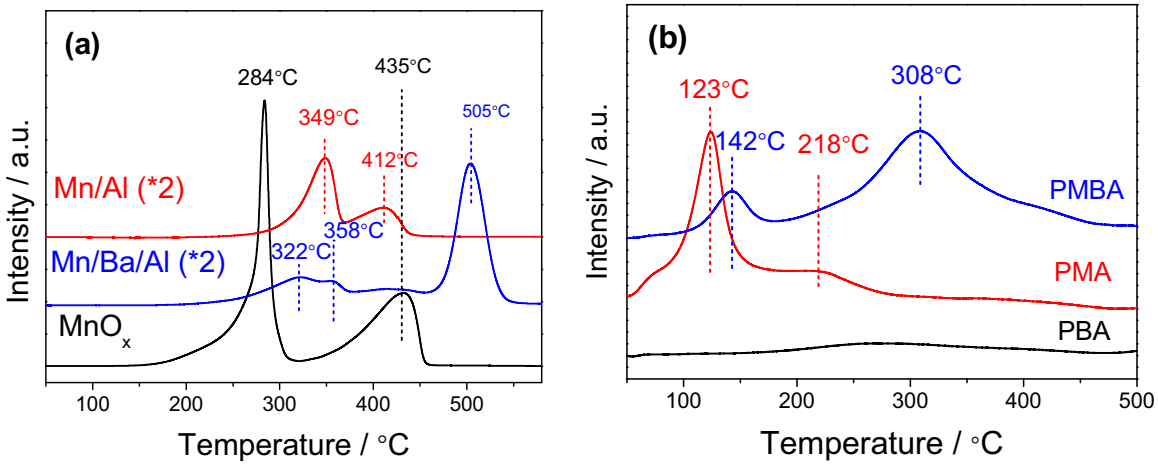

Fig. 2. H_2-TPR profiles of the catalysts.

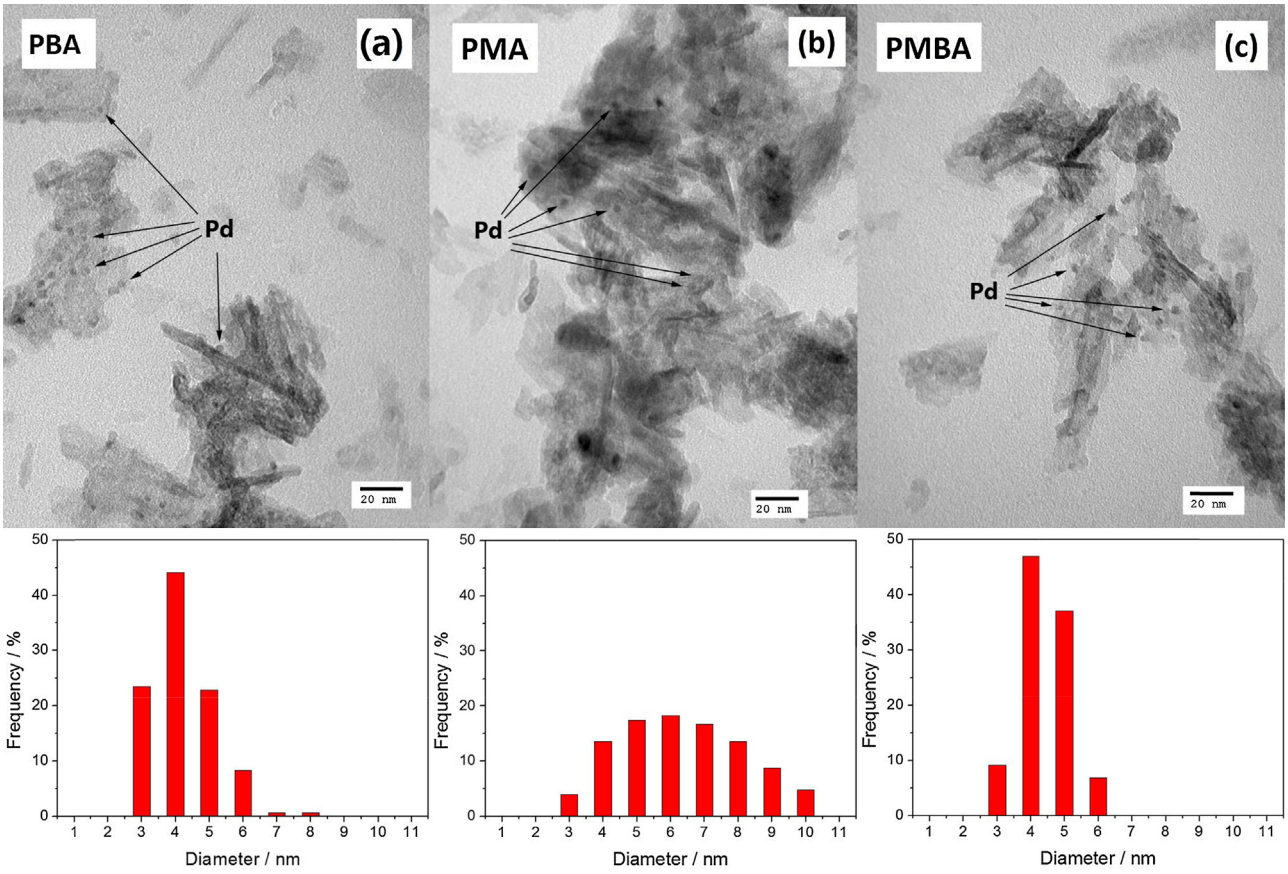

Fig. 3. TEM images and Pd particle size distributions of PBA, PMA and PMBA catalysts.

3.2. NO oxidation capacity

NO oxidation capacity (NOC) was measured at different temperatures over PBA, PMA and PMBA in the absence and presence of H_2O and CO_2. Shown in Fig. 5(a) are the conversions of NO to NO_2 as a function of reaction temperature in the absence of H_2O and CO_2. All samples display a low NOC at 200 °C (<10%). As the temperature rises from 200 to 300 °C, the manganese containing catalysts (PMA and PMBA) showed enhanced NOC, the conversion increasing from 9.1% and 9.6% to 31.5% and 41.3%, respectively. However, the conversion over the PBA catalyst was still quite low (11.6% at 300 °C). Together, these results suggest that the manganese component of catalysts PMA and PMBA contributes significantly to NOC at 300 °C. When the temperature was raised to 400 °C, NO conversion was noticeably increased over PBA, which displayed comparable activity with PMA and PMBA. Indeed, the NO conversion approached the value predicted for thermodynamic NO/NO_2 equilibrium at this temperature (the equilibrium NO conversion, calculated using HSC Chemistry v7.0 software, being shown by the dotted line in Fig. 5). This observation is in line with literature data which show that Pd is generally a poor catalyst for NO oxidation, exhibiting significant activity at elevated temperatures only [22]. Correlating the XPS measurements with the NOC data at 300 °C, it can be surmised that surface adsorbed oxygen plays an important role in NO oxidation [27]; i.e., the manganese-containing catalysts (PMA and PMBA), containing higher amounts

Table 3
Summary of XPS data for prepared catalysts.[a,b]

Catalyst	Atomic concentration (%)				Atomic ratio			
	Pd	Ba	Mn	Al	Pd/Ba	Mn/Al	Pd/Al	Ba/Al
PBA	0.095	4.35	–	23.86	2.18	–	0.40	18.23
PMA	0.077	–	1.45	28.61	–	5.06	0.27	–
PMBA	0.108	4.81	2.44	24.14	2.25	10.14	0.45	19.94

[a] Atomic sensitivity factors taken from Ref. [34].
[b] The denominator of the atomic ratio was corrected to 100 wt%.

Table 4
Binding energies (eV) of core levels and surface valence distribution of the catalysts.

Catalysts	O_{latt}^{2-} (eV)	O_{ads} (eV)	O_{ads}/O_{latt}^{2-}	Mn^{3+} (eV)	Mn^{4+} (eV)	Mn^{4+}/Mn^{3+}
PBA	531.1	532.9	0.105	–	–	–
PMA	530.5	532.0	0.665	641.5	643.8	0.748
PMBA	531.4	532.9	0.270	641.7	642.8	0.496

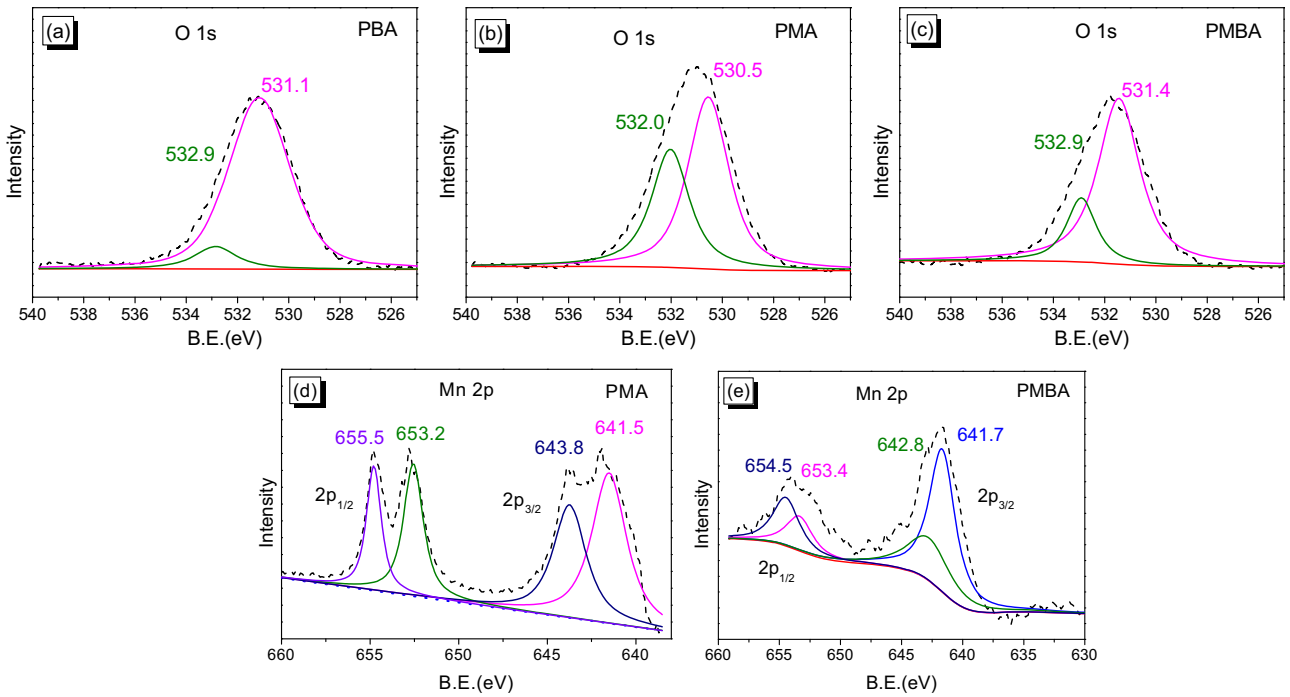

Fig. 4. XPS spectra of PBA, PMA and PMBA catalysts.

of surface oxygen than PBA, exhibit higher NO oxidation capacity.

Fig. 5(b) shows the conversion of NO to NO_2 as a function of reaction temperature in the presence of H_2O and CO_2. For PBA, the addition of H_2O and CO_2 significantly decreased the NOC, particularly at 400 °C (the NO conversion decreasing from 43.3% to 15.8%). However, the NOC was almost unchanged in the case of the PMA catalyst. Compared with PBA, the NOC over PMBA was much higher in the presence of H_2O and CO_2, which is significant for real-world applications.

3.3. NO_x storage capacity

The NO_x storage capacities (NSCs) of the catalysts were measured at 200, 300 and 400 °C in the absence and presence of H_2O and CO_2. The results for storage times of 2 min and 50 min are reported in Table 5 (the NO_x recorded profiles during NSC tests being shown in Fig. S2 in the Supplementary material). For the data collected at 2 min (which are of the most relevance to "real-world" lean-rich cycling conditions), the NSC values span a relatively narrow range, as might be expected given that the catalysts are far from saturation at this relatively short storage time. However, several trends are apparent, namely that: (i) catalyst PMBA displays superior NSC to the other catalysts in the absence/presence at all temperatures; (ii) all of the catalysts reach their maximum NSC at 400 °C, except for PMA which reaches its maximum at 300 °C; and (iii) PMA (containing no Ba) shows the lowest NSC of all the samples at 400 °C. Turning to the 50 min data, it is evident that many of the same trends hold. Indeed, PBA catalyst exhibited its highest NSC value of 695 μmol/g at 400 °C in the absence of H_2O and CO_2, which can be attributed to the fact that the strong surface basicity of BaO imparts relatively high thermal stability to the nitrate [24]. The PMA sample displayed the lowest NSC at all temperatures, indicating that the absence of barium significantly decreased NO_x storage capacity, its poor performance at 400 °C being explained by the poor thermal stability of NO_x stored on the Al_2O_3 support. Note that bulk $Mn(NO_3)_2$ decomposes at <300 °C [36]. The highest NSC value at 200 °C, 300 °C and 400 °C was obtained with PMBA, indicating that the presence of manganese as the main NO oxidation component and barium as the chief NO_x storage component significantly improved NO_x storage capacity at all temperatures, in agreement with the findings of Xiao et al. [37].

Compared to the experiments performed using only $NO/O_2/Ar$ as the feed gas, the addition of H_2O and CO_2 to the feed significantly decreased the NSC for PBA at all temperatures tested. For PMA, the addition of H_2O and CO_2 decreased the NSC at 200 and 300 °C (from 171 and 209 μmol/g to 73 and 121 μmol/g, respectively). However, H_2O and CO_2 had no influence on the NSC at 400 °C, for which the NSC was 109 μmol/g in the presence of H_2O and CO_2 and 108 μmol/g in the absence of H_2O and CO_2. As shown in Table 5, the presence of H_2O and CO_2 greatly reduced the NSC over PMBA also, especially at lower temperatures (≤300 °C), and it should be due to the NO_x adsorption may compete with H_2O and CO_2 adsorption. Furthermore, H_2O also inhibits the oxidation of NO over PMBA at 200 and 300 °C (as shown in Fig. 5). Notably, from the comparison of the NSC data in the presence of H_2O and CO_2 for PBA and PMBA, it is clear that Mn addition greatly enhanced the NSC at higher temperatures (≥300 °C).

Noteworthy, the significant enhancement of the NO_x storage capacity when Mn are added could not only be attributed to an improvement of the NO oxidation rate, but also to an improvement of the proximity between the NO oxidation sites (Mn) and the NO_x storage sites (Ba), which is known to be a key factor for a fast NO_x storage [11,38]. As previously described, the $BaMnO_3$ perovskite is observed for PMBA as shown in XRD patterns (Fig. 1) and the H_2 consumption peaks ascribed to the reduction of $BaMnO_3$ was also detected as shown in H_2-TPR profiles (Fig. 2). Benefitting from the improvement of the proximity between the NO oxidation sites and the NO_x storages sites, and Mn could participate to the NO_x species diffusion, in addition with the enhancement of the NO into NO_2 oxidation activity.

3.4. Thermal stability of stored NO_x

After exposing the PBA, PMA and PMBA samples to a $NO/O_2/Ar$ mixture for 50 min at 200 °C, the thermal stability of the stored NO_x

Table 5
NO_x storage capacities (NSCs) measured under lean conditions (500 ppm NO, 8% O_2, with or without 2% CO_2 and 2% H_2O, N_2 balance, 2 min or 50 min storage, GHSV = 100,000 h^{-1}).

Catalyst code	NO_x storage capacity (μmol/g)					
	$NO + O_2/NO + O_2 + CO_2 + H_2O$ (2 min)			$NO + O_2/NO + O_2 + CO_2 + H_2O$ (50 min)		
	200 °C	300 °C	400 °C	200 °C	300 °C	400 °C
PBA	27.2/11.7	23.4/16.8	28.0/18.7	329/225	474/292	695/348
PMA	20.7/19.4	24.6/21.4	14.9/10.3	171/73	209/121	108/109
PMBA	27.0/16.1	32.8/22.6	33.4/26.3	574/165	775/467	785/472

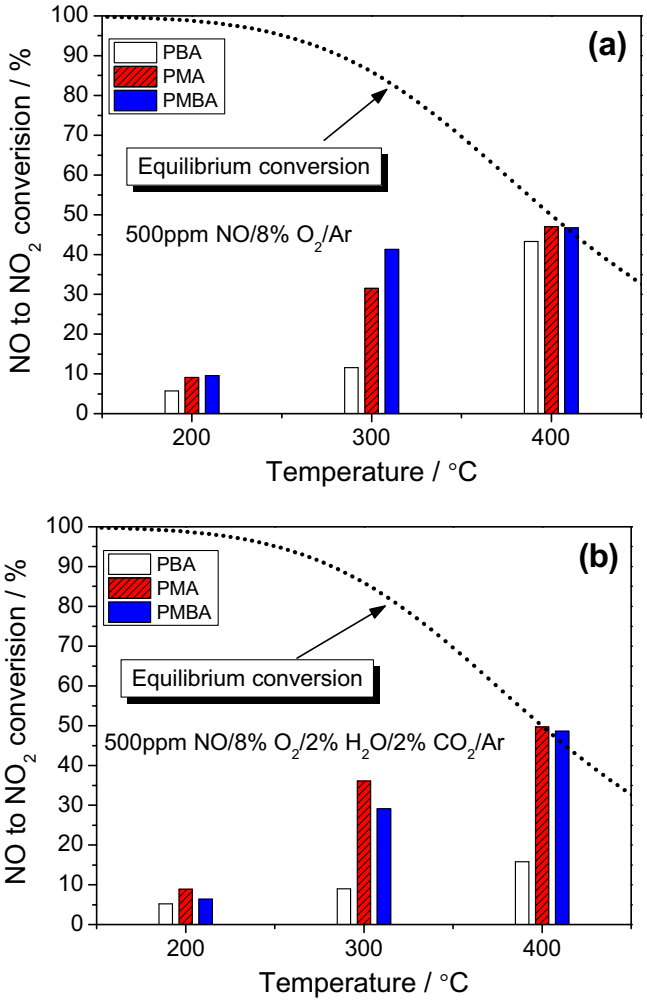

Fig. 5. NO conversion to NO_2 measured under lean conditions (500 ppm NO, 8% O_2, with or without 2% CO_2 and 2% H_2O, Ar balance, GHSV = 100,000 h^{-1}) without H_2O and CO_2 (a) and with H_2O and CO_2 (b).

was investigated by means of NO_x-TPD experiments conducted in a high purity argon flow, the results being shown in Fig. 6. For the PBA sample (Fig. 6(a)), two obvious NO_x desorption peaks (m/z = 30) were observed at 332 and 495 °C (note that the m/z = 30 signal can result from desorption of NO and/or NO_2 due to the fragmentation of NO_2 to NO in the mass spectrometer [39]). The low temperature peak can be attributed to NO_x adsorbed on the Al_2O_3 support or species nearby metal sites [3], while the later peak, which was accompanied by O_2 (m/z = 32) formation, can be assigned to the decomposition of nitrate or nitrite at Ba sites [35,40]. In general, very little NO_2 (m/z = 46) was observed during TPD for the different samples, a fact which can be attributed, at least in part, to NO being the favored species with respect to the thermodynamic equilibrium between NO and NO_2 at high temperatures (≥400 °C) [14]. In the case of PMA, a NO_x desorption peak (m/z = 30) was observed at 311 °C as shown in Fig. 6(b), indicative of the poor thermal stability of NO_x stored on the PMA sample; moreover, a small NO_2 desorption peak (m/z = 46, see inset of Fig. 6(b)) was also observed at this temperature. For the PMBA sample, two obvious NO_x desorption peaks were observed at 310 and 440 °C. Based on the results of NO_x desorption from PBA and PMA, it is reasonable to ascribe the peak at low temperature to weakly adsorbed NO_x, and the high temperature peak to NO_x adsorbed on BaO. However, compared with NO_x desorption from PBA, the desorption of NO_x adsorbed on Ba shifted to lower temperatures due to the incorporation of Mn.

TPD experiments were also conducted over the PBA, PMA, and PMBA samples in which H_2O and CO_2 were added to the NO/O_2 feed during NO_x storage. Compared with the experiments in which H_2O and CO_2 were absent, the intensities of the NO_x desorption peaks significantly decreased, which is in accordance with the finding that NSC is decreased in the presence of H_2O/CO_2 (Table 5). In addition, the NO_x desorption peaks shifted to higher temperatures when storage was performed in the presence of H_2O and CO_2. According to work by Theis et al. [41], the presence of H_2O enhances the spillover of NO_2 from Pt sites to the NO_x storage sites during lean operation, possibly by the formation of nitric acid (HNO_3) which then reacts with NO_x storage sites to form the stored NO_x species. Consequently, it can be speculated that the higher NO_x mobility in the presence of H_2O results in NO_x storage at sites further away from Pt, which might explain the higher desorption temperature.

Fig. 5(d)–(f) also show CO_2 evolution traces recorded during TPD measurements. Sharp CO_2 generation signals appeared above 600 °C over PBA and PMBA samples, which should be related to the decomposition of bulk $BaCO_3$ at elevated temperatures. While the CO_2 release in the low temperature region should come from the decomposition of surface unidentates and bidentates barium carbonate species. It is noted that the temperatures for decomposition of surface and bulk carbonates were both lower over PMBA compared with those of PBA, indicating the synergistic effect between Mn and Ba for decomposition of the carbonates here.

3.5. NO_x species studied by in situ DRIFTS

DRIFTS spectra showing the evolution of surface NO_x species at different temperatures are shown in Fig. 7. After exposing the $Pd/Ba/Al_2O_3$ catalyst to a 500 ppm NO/8% O_2/Ar mixture for 30 min at 200 °C, an obvious band at 1230 cm^{-1} and a small band at 1585 cm^{-1} were observed (Fig. 7(a)). The band at 1230 cm^{-1} can be attributed to bridged nitrite species on Ba or on Al sites [42,43], while the band at 1585 cm^{-1} can be similarly be assigned to bridged nitrates on Ba and/or bridged nitrates on Al in close proximity to Ba [43]. Upon exposure of the PBA sample to the same atmosphere at 300 °C, the initially formed band at band at 1230 cm^{-1} gradually decreased in intensity and overlapped with a new band at 1305 cm^{-1}. Meanwhile the band centered at 1585 cm^{-1} gradually increased in intensity. The new band at 1305 cm^{-1} is assigned to monodentate nitrates associated with Ba [43]. When the same experiment was carried out at 400 °C, nitrites on Ba (1230 cm^{-1}) were no longer observed and the Ba nitrate band at 1305 cm^{-1} was

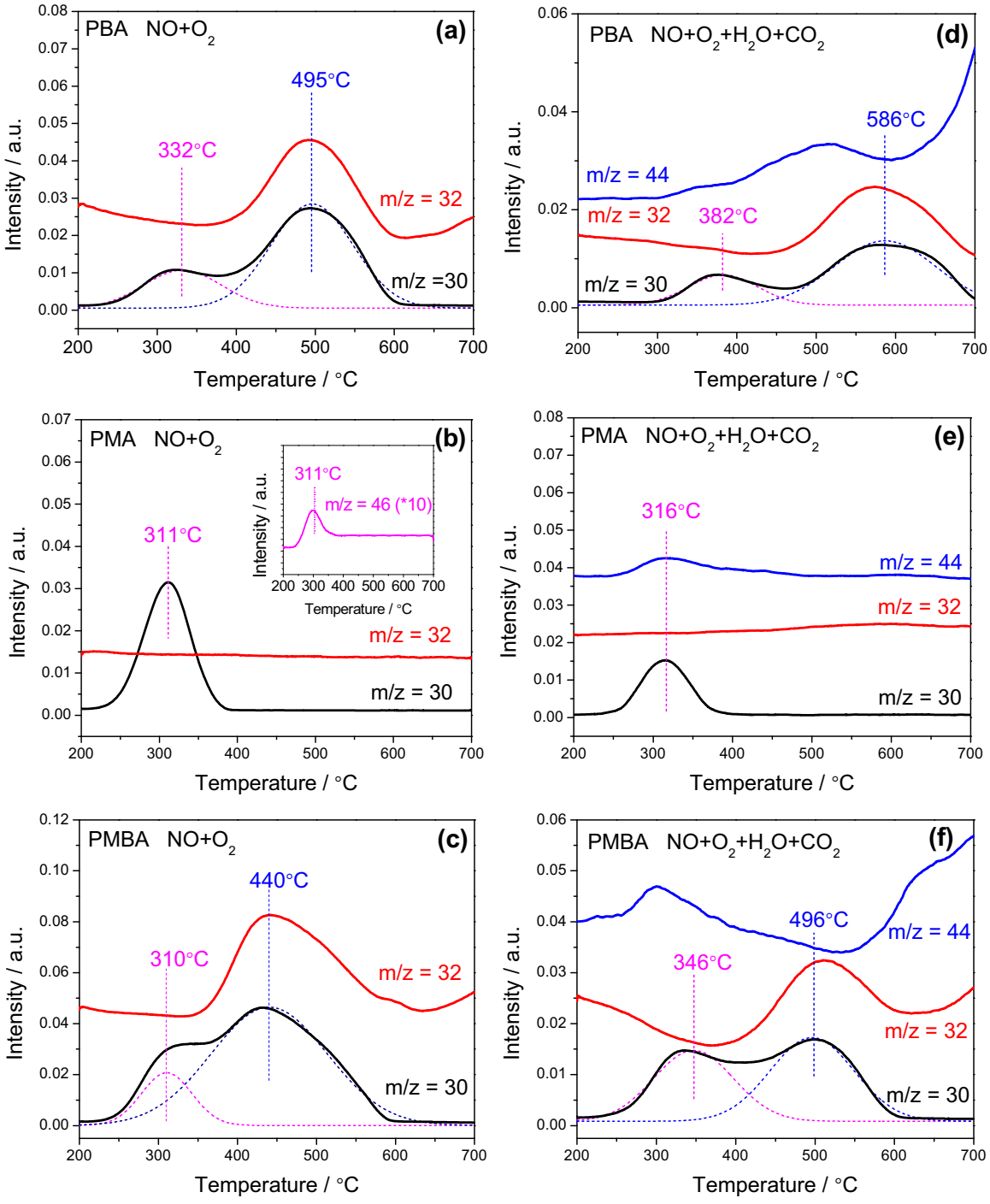

Fig. 6. Evolution of NO_x, CO_2 and O_2 during NO_x-TPD experiments. The samples were kept under 500 ppm NO/8% O_2/Ar with or without 2% H_2O and 2% CO_2 for 60 min at 200 °C. After Ar purging at 200 °C for 30 min, the temperature was increased to 700 °C at 10 °C/min under Ar flow.

the dominant species in the spectrum after 30 min of NO_x adsorption.

Exposure of the PMA sample to a 500 ppm NO/8% O_2/Ar mixture at 200 °C (Fig. 7(b)) resulted in the appearance of two distinct bands at 1230 and 1300 cm^{-1} which can be assigned to bridged nitrite and nitrate species on Al or Mn sites, although the precise assignment of these bands is difficult due to the considerable number of species which absorb in this region [44–46]. Upon exposure to the NO/O_2/Ar gas stream at 300 °C, a strong band at 1552 cm^{-1} and a weak band at 1300 cm^{-1} were observed. The former can be assigned to monodentate nitrate species on Al [47], while the latter can be attributed to bidentate nitrate species on Mn or Al [42,44,48–50]. Upon heating to 400 °C, the spectrum obtained was very similar to that at 300 °C, the great majority of NO_x being present in form of nitrate on the PMA surface. It is worth noting that the intensity of the bands at 1552 and 1300 cm^{-1} was significantly decreased at 400 °C, which is indicative of the poor thermal stability of NO_x stored on the PMA sample (Fig. 6(b)).

Finally, for the PMBA catalyst, after exposure to the NO/O_2/Ar mixture for 30 min at 200 °C (Fig. 7(c)), NO_x was present chiefly as bridged nitrite species on Ba (1230 cm^{-1}) [42–45], while the band due to monodentate nitrate on Ba (1315 cm^{-1}) [43] was very

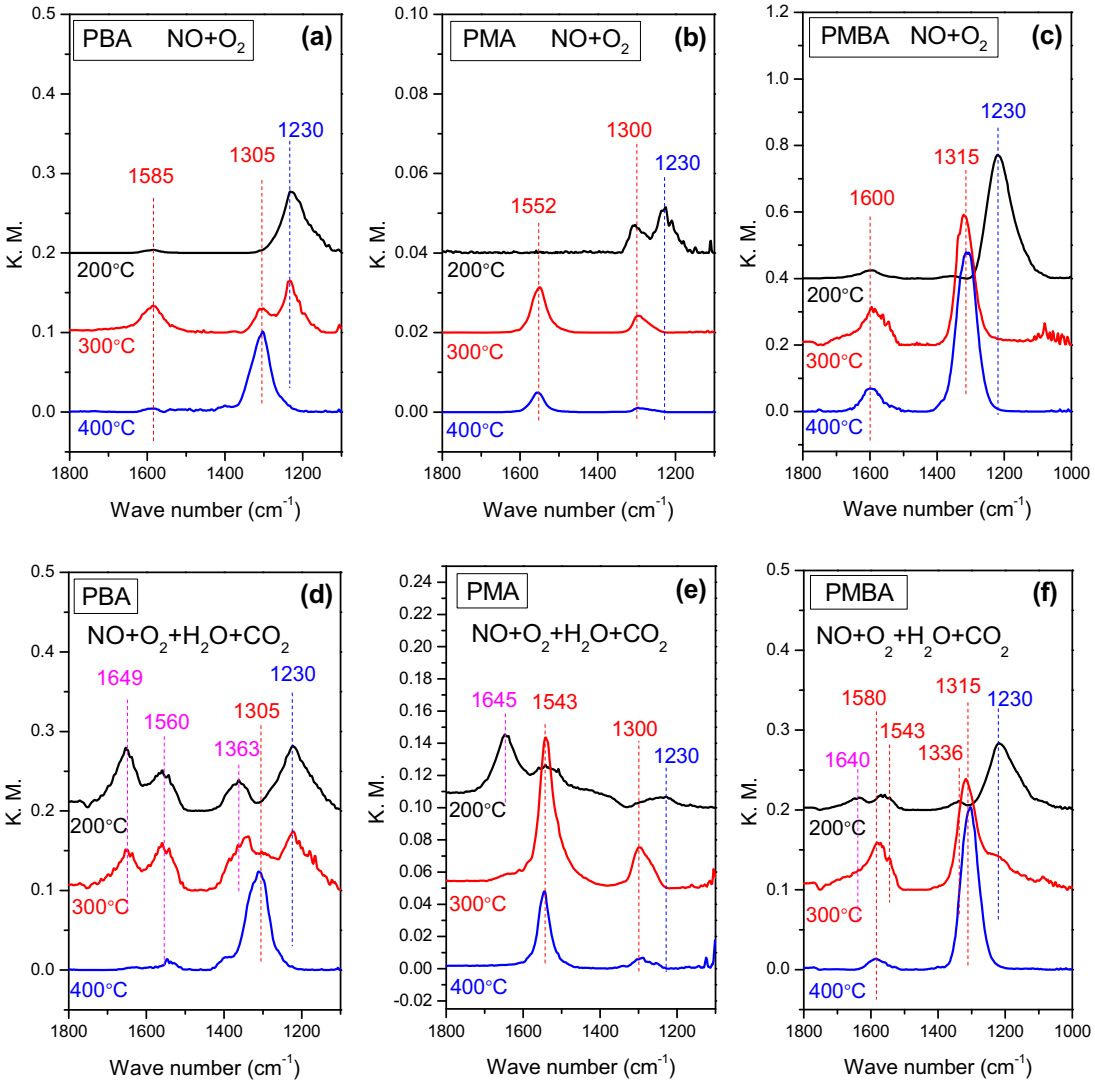

Fig. 7. In situ DRIFTS spectra of PBA, PMA and PMBA catalysts after 30 min NO adsorption at different temperatures.

weak. At 300 °C, the main surface species corresponded to monodentate nitrates on Ba (1315 cm^{-1}) and bridging nitrates on Ba or Al (1600 cm^{-1}) [43,45]. In contrast, nitrites could be observed on the surface of PBA at this temperature (Fig. 7(a)). This discrepancy can be attributed to the higher NO oxidation activity of PMBA compared to PBA. With further increase of the temperature to 400 °C, the spectrum was similar to that obtained at 300 °C, NO_x existing mainly in the form of nitrates on the catalyst.

When H_2O and CO_2 were introduced into the feed gas, the results obtained were somewhat different as shown in Fig. 7(d)–(f). At 200 °C strong bands centered at ca. 1363 cm^{-1} and 1560 cm^{-1} were observed for the three samples which can be assigned to carbonates on barium, as well as a band due to adsorbed water δ(H–O–H) [51] at ca.1649 cm^{-1}. Upon heating to 300 °C, the carbonate and H_2O bands decreased in intensity although were still present for the PBA and PMBA samples. Notably, only bands ascribed to the nitrites/nitrates appeared on PMA at 300 °C, while no bands due to carbonates could be detected. Upon further increase of the temperature to 400 °C, there were no bands attributable to adsorbed carbonates and H_2O for any of the samples, only strongly bonded nitrate species being left on the surface. These results indicate that carbonate species are less stable than nitrates, the competitive adsorption of CO_2 with NO_x being negligible at 400 °C for PBA and PMBA, and at 300 °C for PMA.

The thermal stability of the carbonates on PBA and PMA was also studied by DRIFTS, the results of these measurements being shown in Fig. S1 in the Supplementary material. H_2O and CO_2 were first adsorbed by exposing the samples to flowing 2% H_2O/2% CO_2/Ar at 50 °C for 30 min, after which the system was flushed with Ar and a series of spectra were collected under Ar at increasing temperature. The bands due to carbonates and adsorbed H_2O decreased in intensity with increase of the exposure temperature, the peaks being very weak at 200 °C for PBA. In the case of PMA, only very weak bands due to carbonates could be observed at 150 °C.

3.6. NO_x storage and reduction

NO_x storage and reduction were also investigated under cycling conditions, in both the absence and presence of H_2O and CO_2; the results of these experiments are depicted in Fig. 8. Note that NO_x conversion refers to the conversion of NO_x to reduction products, i.e., N_2, NH_3 and N_2O. Fig. 8(a) depicts the cycled-averaged NO_x conversions as a function of reaction temperature, measured in the absence of H_2O and CO_2. For the PBA catalyst, the NO_x removal efficiency increased with increasing temperature and the highest conversion was obtained at 400 °C, which is consistent with results reported in the literature [52]. Over PMA, the highest NO_x conversion was obtained at 300 °C, which is likely related to the poor

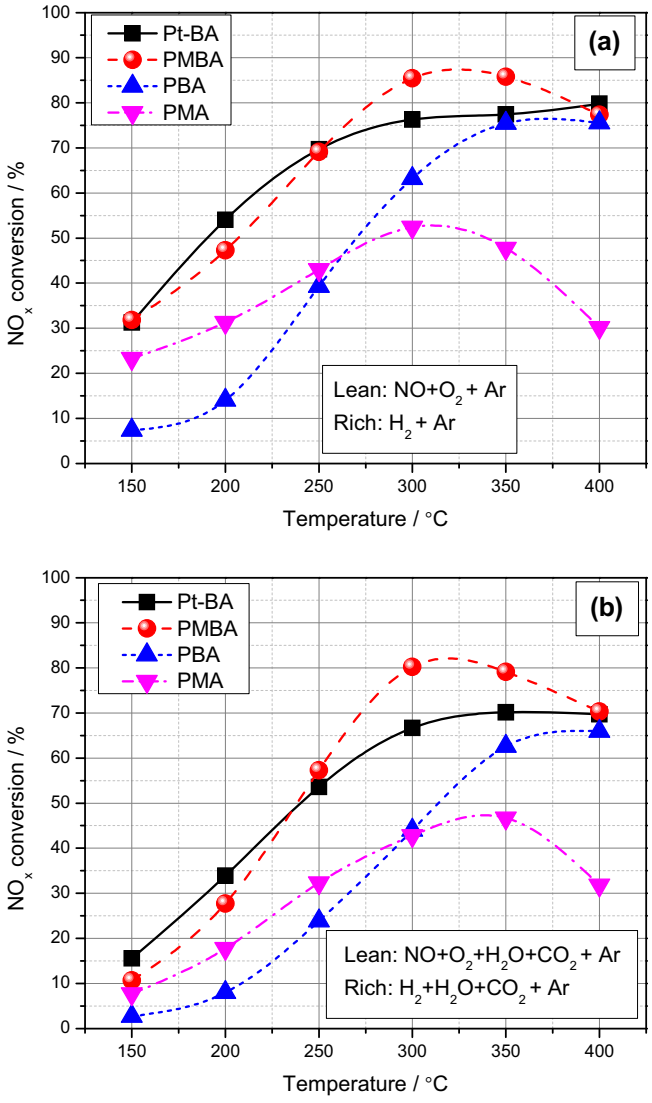

Fig. 8. NO_x conversion of PBA, PMA, PMBA and Pt/20Ba/Al_2O_3 ("Pt-BA") under cyclic lean-rich conditions at different temperatures. Lean (120 s): 500 ppm NO, 8% O_2, with or without 2% CO_2 and 2% H_2O, Ar balanced; Rich (10 s): 1% H_2, with or without 2% CO_2 and 2% H_2O, Ar as balance, GHSV = 30,000 h^{-1}.

thermal stability of the stored NO_x on Al or Mn (as indicated by the NO_x-TPD and in situ DRIFTS results shown in Figs. 6 and 7). In the case of PMBA, considerably higher cycle-averaged NO_x conversions were obtained at 200–400 °C compared to the PBA and PMA catalysts. This is largely due to the higher activity of PMBA for NO oxidation to NO_2 (Fig. 5), which is one of the drawbacks of Pd compared with Pt [22]. The poor performance of the PMA catalyst in comparison further emphasizes the key role of the Ba NO_x storage phase, as highlighted by the NSC data (Table 5). Significantly, PMBA displayed comparable activity to a traditional LNT catalyst of the Pt/20BaO/Al_2O_3 type (denoted by the sample code Pt-BA, corresponding to the solid black line in Fig. 8(a)); indeed, PMBA afforded slightly higher cycle-averaged NO_x conversions in the range 300–350 °C. The NSC for PBA and PMBA samples reached its highest value at 400 °C as shown in Table 5, this result can be attributed to the fact that NO_x is mainly stored as nitrate on Ba, the kinetics of NO oxidation to NO_2 being favored at the higher temperature. Furthermore, the basic nature of Ba imparts relatively high thermal stability to the nitrate. For LNT catalysts, the cycle-averaged NO_x removal efficiency is dependent on the lean phase NO_x storage efficiency and rich phase NO_x reduction efficiency. Under rich phase, NO_x from barium nitrites or nitrates are reduced to N_2 on Pt or Pd surface by H_2, CO, and/or hydrocarbons from the rich exhaust gas. Therefore, to achieve a better NO_x removal efficiency during rich phase, there need to have balance between the rates of nitrate decomposition and NO_x reduction. At 400 °C, the rate of nitrate decomposition was higher than that of NO_x reduction, resulting in significant NO_x slip (without reduction), which reduces NO_x removal efficiency. The intermediate temperature of 300–350 °C represents an optimum at which a balance is achieved between the rates of nitrate decomposition and NO_x reduction. Therefore, the optimum is 300–350 °C for traditional Pt-based LNT catalysts.

This result serves to emphasize the potential of Mn for replacing Pt in LNT catalysts, albeit that in real world applications the extent to which Pt can be replaced will depend on additional factors such as catalyst durability and the extent to which Mn-containing catalysts can be desulfated at low/zero Pt loadings.

When H_2O and CO_2 were added to the feed gas (Fig. 8(b)), PBA exhibited decreased NO_x removal efficiency at all temperatures. This is mainly due to the fact that the NO_x storage capacity on PBA is significantly inhibited by the addition of H_2O and CO_2 [3,40,53]. Notably, the presence of H_2O and CO_2 in the feed did not decrease the NO_x conversion of PMA as much as that of PBA. Indeed, similar NO_x conversion was observed in the presence of H_2O and CO_2 (30.2%) at 400 °C to that obtained in the absence of H_2O and CO_2 (31.8%). This result is in accordance with NSC measurements (Table 5), in which similar NSC was obtained for PMA at 400 °C in the presence or absence of H_2O and CO_2. As shown by the DRIFTS results (Fig. 7(e)), there were almost no carbonate species formed on the PMA catalyst during NO_x storage in the presence of H_2O and CO_2 above 300 °C, which can been attributed to the facile decomposition of manganese carbonate [21]. Consequently, the presence of CO_2 had no influence on the NO_x storage and reduction ability of the PMA catalyst at higher temperatures (≥300 °C). In the case of PMBA, NO_x conversions were decreased in the presence of H_2O and CO_2, which is in agreement with the NSC data shown in Table 5. However, compared with PBA, it is obvious that PMBA shows improved tolerance toward CO_2 and H_2O. Again, this can be rationalized by the fact that the carbonates on Mn are decomposed at temperatures close to 200 °C (Fig. 7(f)), which is not the case for Ba [54].

The NO_x concentration profiles under cycling being shown in Fig. 9, the cycle-averaged lean phase NO_x storage efficiency and rich phase NO_x release are collected in Table 6. Catalyst performance during the lean phase can be evaluated in terms of the NO_x storage efficiency (NSE), defined as the amount of NO_x stored divided by the total amount of NO_x supplied to the catalyst during the lean phase (120 s).

Rich phase performance can be characterized in terms of the percentage of NO_x released (NRE), i.e., the amount of NO_x released during the rich phase – without reduction – divided by the total amount of NO_x stored during the lean phase. Rich phase NO_x release is dependent on the rates of four processes [3]: reductant delivery, nitrate decomposition, consumption of stored oxygen and NO_x reduction. From this, it follows that for a given set of conditions it is important to establish a balance between nitrate decomposition and NO_x reduction. In this study, for each sample the lowest NO_x release percentage was observed at 300 °C. The comparatively higher NO_x release at 200 °C can be ascribed to an imbalance between the rates of nitrate decomposition and NO_x reduction, i.e., the rate of NO_x reduction was too slow for the liberated NO_x to be fully consumed. At 400 °C, the thermal instability of the nitrates was such that the rate of nitrate decomposition was also much higher than that of NO_x reduction (even though the latter should be fast at this temperature), resulting in significant NO_x slip, especially for PMA catalyst. The intermediate temperature of 300 °C therefore

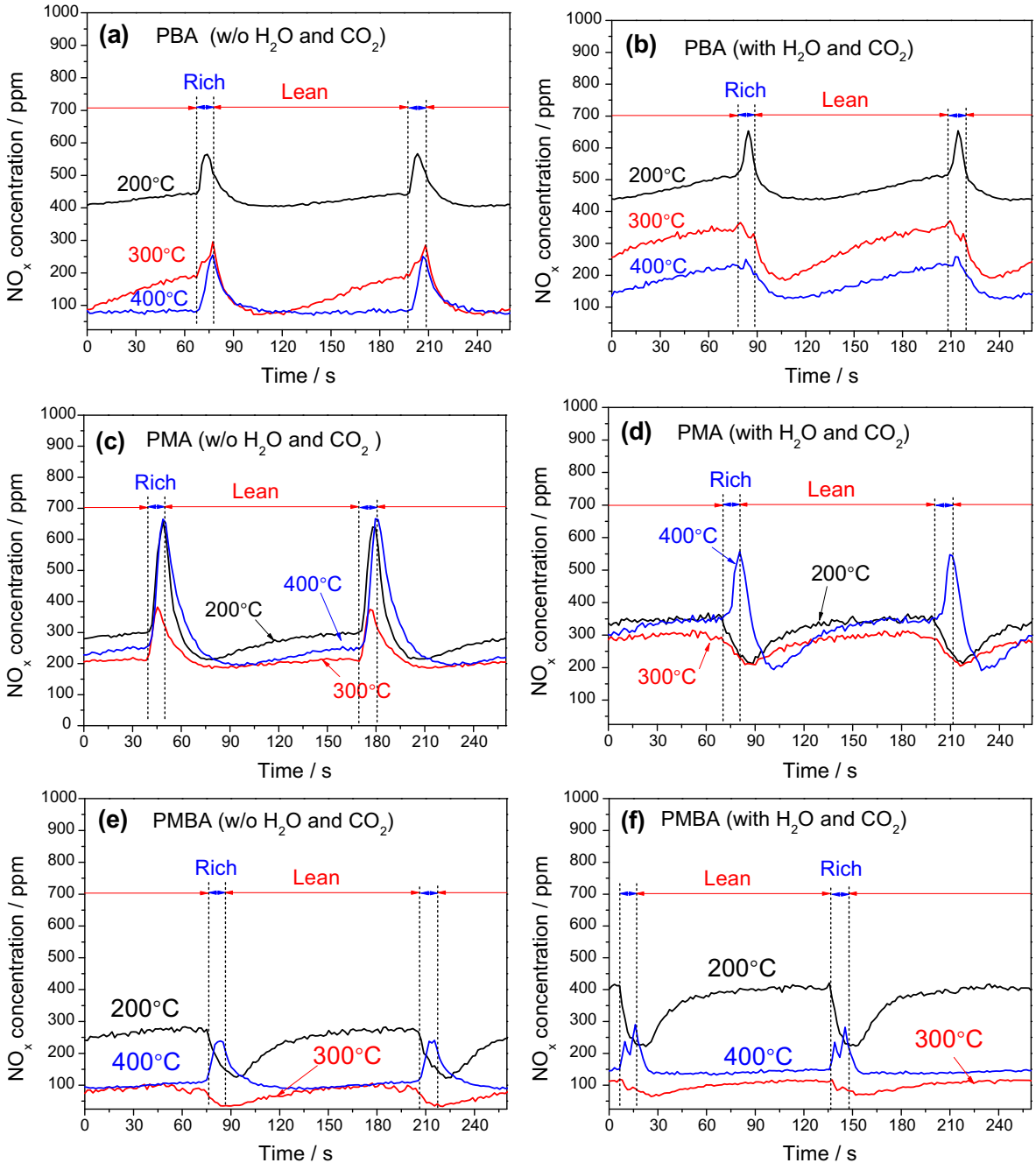

Fig. 9. NO_x concentration profiles during lean-rich cycling at 200, 300 and 400 °C. See Table 1 for experimental conditions.

represents an optimum at which a balance is achieved between the rates of nitrate decomposition and NO_x reduction.

3.7. Product selectivity during regeneration

NO_x reduction product speciation during regeneration has been investigated, the results being shown in Table 7. The reduction of stored nitrates and nitrites leads to the formation of different nitrogen containing species, such as N_2, NH_3 and N_2O along with H_2O. The objective of the NSR operation is to maximize the conversion of NO into N_2, avoiding the formation of NH_3 and N_2O as far as possible. The reduction of stored nitrates with hydrogen has been found to occur by the following reactions:

$$Ba(NO_3)_2 + 5H_2 \rightarrow N_2 + BaO + 5H_2O \quad (4)$$

$$Ba(NO_3)_2 + 8H_2 \rightarrow 2NH_3 + BaO + 5H_2O \quad (5)$$

$$Ba(NO_3)_2 + 4H_2 \rightarrow N_2O + BaO + 4H_2O \quad (6)$$

$$N_2O + H_2 \rightarrow N_2 + H_2O \quad (7)$$

$$Ba(NO_3)_2 + 10NH_3 \rightarrow 8N_2 + 3BaO + 15H_2O \quad (8)$$

For all samples (in the absence/presence of H_2O and CO_2, as shown in Table 7), NH_3 and N_2O were both observed during the regeneration phase, and at significant levels at low temperature (200 °C). Primarily attributed to that during reduction of stored nitrates at 200 °C, reactions (5) and (6) accounted for the NO_x reduction. Formation of NH_3 and N_2O decreased with increasing temperatures and can be neglected at 400 °C, mainly due to N_2 formation was promoted due to reactions (7) and (8) where the formed NH_3 and N_2O continued to react further with stored nitrates or H_2

Table 6
Comparison of NO_x storage and release during NO_x storage/reduction cycling.[a]

Temperature (°C)	Catalyst	NO_x conversion (%)	NSC (120 s) (μmol/g)	NO_x release (μmol/g)	NSE (%)	NRE (%)[b]
200 (w/o H_2O/CO_2)	PBA	14.0	7.18	2.18	20.1	30.3
	PMA	31.3	13.07	1.95	36.6	14.9
	PMBA	47.3	18.82	1.92	52.7	10.2
300 (w/o H_2O/CO_2)	PBA	63.2	24.39	1.54	68.3	6.3
	PMA	52.4	22.00	3.19	61.6	14.5
	PMBA	85.5	32.39	1.85	90.7	5.7
400 (w/o H_2O/CO_2)	PBA	75.5	28.79	2.16	80.6	7.5
	PMA	30.2	16.75	5.95	46.9	35.6
	PMBA	77.4	30.96	3.31	86.7	10.7
200 (w/H_2O/CO_2)	PBA	8.0	5.00	2.14	14.0	42.8
	PMA	17.7	7.43	1.10	20.8	14.8
	PMBA	27.8	11.82	1.88	33.1	15.9
300 (w/H_2O/CO_2)	PBA	44.0	17.57	0.67	49.2	3.8
	PMA	42.8	17.50	2.21	49.0	12.6
	PMBA	80.2	30.68	2.02	85.9	6.6
400 (w/H_2O/CO_2)	PBA	65.9	24.46	2.59	68.5	10.6
	PMA	31.8	14.61	3.26	40.9	22.3
	PMBA	70.3	28.07	2.98	78.6	10.6

[a] "w/o" means "without", "w" means "with".
[b] (NO_x released in rich purge/NO_x stored in lean phase) × 100%.

Table 7
Selectivity of N_2, NH_3 and N_2O during NO_x storage/reduction cycling.[a]

Temperature (°C)	Catalyst	N_2 selectivity (%)	NH_3 selectivity (%)	N_2O selectivity (%)
200 (w/o H_2O/CO_2)	PBA	50	34	16
	PMA	68	18	14
	PMBA	89	4	7
300 (w/o H_2O/CO_2)	PBA	80	14	6
	PMA	90	5	5
	PMBA	94	2	4
400 (w/o H_2O/CO_2)	PBA	92	4	4
	PMA	91	3	6
	PMBA	97	1	2
200 (w/H_2O/CO_2)	PBA	66	18	16
	PMA	78	13	9
	PMBA	88	7	5
300 (w/H_2O/CO_2)	PBA	89	3	8
	PMA	97	2	1
	PMBA	91	5	4
400 (w/H_2O/CO_2)	PBA	91	6	3
	PMA	96	4	0
	PMBA	96	2	2

[a] "w/o" means "without", "w" means "with".

to form nitrogen, which is consistent with results reported in the literature [55].

Notably, from the comparison of the selectivity data (in the absence/presence of H_2O and CO_2) for PBA, PMA and PMBA, it is clear that Mn addition greatly decreased the NH_3 selectivity, especially at low temperatures. This can be attributed to the enhanced $NH_3 + NO + NO_2 \rightarrow N_2 + H_2O$ activity associated with the Mn phase [12]. Benefitting from this improved N_2 selectivity and enhanced NO_x storage capacity, PMBA catalyst displayed excellent NSR performance.

4. Conclusions

Manganese-containing LNT catalysts were prepared and found to exhibit higher activity for NO oxidation to NO_2 than a Pd/Ba/Al reference catalyst. Moreover, compared to the Pd/Ba/Al reference, a Pd/Mn/Ba/Al catalyst was shown to achieve significantly improved NO_x conversion under lean-rich cycling conditions. This is attributed to its increased activity for NO oxidation, which, combined with the presence of Ba, results in high NO_x storage efficiency. In addition, the presence of Mn greatly lessened the inhibiting effects of H_2O and CO_2 on cycle-averaged NO_x conversion, this being due to the facile decomposition of manganese carbonate at low temperatures as evidenced by DRIFTS. Significantly, the Pd/Mn/Ba/Al catalyst displayed comparable activity to a traditional LNT catalyst of the Pt/Ba/Al type. This result serves to emphasize the potential of Mn for replacing Pt in LNT catalysts, albeit that in real world applications the extent to which Pt can be replaced will depend on additional factors such as catalyst durability.

Acknowledgments

The work was supported by the National Natural Science Foundation of China (Nos. 21373037, 21073024 and 21176037). MC thanks the National Science Foundation and the U.S. Department of Energy (DOE) for financial support under award no. CBET-1258742.

However, any opinions, findings, conclusions, or recommendations expressed herein are those of the authors and do not necessarily reflect the views of the DOE.

Appendix A. Supplementary data

Supplementary data associated with this article can be found, in the online version, at http://dx.doi.org/10.1016/j.apcatb.2014.10.001.

References

[1] P. Granger, V.I. Parvulescu, Chem. Rev. 111 (2011) 3155–3207.
[2] N. Takahashi, H. Shinjoh, T. Iijima, T. Suzuki, K. Yamazaki, K. Yokota, H. Suzuki, N. Miyoshi, S. Matsumoto, T. Tanizawa, T. Tanaka, S. Tateishi, K. Kasahara, Catal. Today 27 (1996) 63–69.
[3] W.S. Epling, L.E. Campbell, A. Yezerets, N.W. Currier, J.E. Parks, Catal. Rev. 46 (2004) 163–245.
[4] S. Roy, A. Baiker, Chem. Rev. 109 (2009) 4054–4091.
[5] M. Piacentini, M. Maciejewski, A. Baiker, Appl. Catal. B: Environ. 59 (2005) 187–195.
[6] E. Fridell, M. Skoglundh, B. Westerberg, S. Johansson, G. Smedler, J. Catal. 183 (1999) 196–209.
[7] R. Vijay, C.M. Snively, J. Lauterbach, J. Catal. 243 (2006) 368–375.
[8] R. Vijay, R.J. Hendershot, S.M. Rivera-Jiménez, W.B. Rogers, B.J. Feist, C.M. Snively, J. Lauterbach, Catal. Commun. 6 (2005) 167–171.
[9] Y.Y. Ji, C. Fisk, V. Easterling, U. Graham, A. Poole, M. Crocker, J.S. Choi, W. Partridge, K. Wilson, Catal. Today 151 (2010) 362–375.
[10] N. Le Phuc, X. Courtois, F. Can, S. Royer, P. Marecot, D. Duprez, Appl. Catal. B: Environ. 102 (2011) 362–371.
[11] N. Le Phuc, X. Courtois, F. Can, S. Royer, P. Marecot, D. Duprez, Appl. Catal. B: Environ. 102 (2011) 353–361.
[12] P.N. Le, E.C. Corbos, X. Courtois, F. Can, S. Royer, P. Marecot, D. Duprez, Top. Catal. 52 (2009) 1771–1775.
[13] J.H. Xiao, X.H. Li, S. Deng, F.R. Wang, L.F. Wang, Catal. Commun. 9 (2008) 563–567.
[14] W.B. Li, X.F. Yang, L.F. Chen, J.A. Wang, Catal. Today 148 (2009) 75–80.
[15] L.S. Wei, J.H. Li, X.F. Tang, Catal. Lett. 127 (2009) 107–112.
[16] Q.A. Li, M. Meng, H. Xian, N. Tsubaki, X.G. Li, Y.N. Xie, T.D. Hu, J. Zhang, Environ. Sci. Technol. 44 (2010) 4747–4752.
[17] Q. Li, M. Meng, F.F. Dai, Y.Q. Zha, Y.N. Xie, T.D. Hu, J. Zhang, Chem. Eng. J. 184 (2012) 106–112.
[18] H.Y. Huang, R.T. Yang, Langmuir 17 (2001) 4997–5003.
[19] Y.X. Zhang, D.S. Liu, M. Meng, Z. Jiang, S. Zhang, Ind. Eng. Chem. Res. 53 (2014) 8416–8425.
[20] C.H. Kim, G.S. Qi, K. Dahlberg, W. Li, Science 327 (2010) 1624–1627.
[21] X. Kong, Appl. Chem. Ind. 38 (2009) 990–993.
[22] G.W. Graham, H.W. Jen, O. Ezekoye, R.J. Kudla, W. Chun, X.Q. Pan, R.W. McCabe, Catal. Lett. 116 (2007) 1–8.
[23] S. Salasc, M. Skoglundh, E. Fridell, Appl. Catal. B: Environ. 36 (2002) 145–160.
[24] C. Shi, Y. Ji, U.M. Graham, G. Jacobs, M. Crocker, Z. Zhang, Y. Wang, T.J. Toops, Appl. Catal. B: Environ. 119–120 (2012) 183–196.
[25] B.R. Strohmeier, D.M. Hercules, J. Phys. Chem. 88 (1984) 4922–4929.
[26] R. Strobel, M. Maciejewski, S.E. Pratsinis, A. Baiker, Thermochim. Acta 445 (2006) 23–26.
[27] C. Shi, Y. Wang, A. Zhu, B. Chen, C. Au, Catal. Commun. 28 (2012) 18–22.
[28] X.F. Tang, Y.G. Li, X.M. Huang, Y.D. Xu, H.Q. Zhu, J.G. Wang, W.J. Shen, Appl. Catal. B: Environ. 62 (2006) 265–273.
[29] S.H. Liang, F.T.G. Bulgan, R.L. Zong, Y.F. Zhu, J. Phys. Chem. C 112 (2008) 5307–5315.
[30] X. Wang, Y.C. Xie, Catal. Lett. 72 (2001) 51–57.
[31] X.F. Tang, J.L. Chen, X.M. Huang, Y. Xu, W.J. Shen, Appl. Catal. B: Environ. 81 (2008) 115–121.
[32] S. Hamoudi, A. Sayari, K. Belkacemi, L. Bonneviot, F. Larachi, Catal. Today 62 (2000) 379–388.
[33] S.Y. Huang, C.B. Zhang, H. He, J. Environ. Sci. China 25 (2013) 1206–1212.
[34] C. Wagner, D. Briggs, Practical Surface Analysis, 2nd ed., John Wiley and Sons, 1990.
[35] C. Shi, Z.S. Zhang, M. Crocker, L. Xu, C.Y. Wang, C.T. Au, A.M. Zhu, Catal. Today 211 (2013) 96–103.
[36] P.K. Gallagher, F. Schrey, B. Prescott, Thermochim. Acta 2 (1971) 405–412.
[37] J.H. Xiao, X.H. Li, S. Deng, F.R. Wang, L.F. Wang, Chin. Chem. Lett. 17 (2006) 1357–1360.
[38] B. Pereda-Ayo, R. Lopez-Fonseca, J.R. Gonzalez-Velasco, Appl. Catal. A: Gen. 363 (2009) 73–80.
[39] D.H. Kim, K. Mudiyanselage, J. Szanyi, J.C. Hanson, C.H.F. Peden, J. Phys. Chem. C 118 (2014) 4189–4197.
[40] A. Lindholm, N.W. Currier, E. Fridell, A. Yezerets, L. Olsson, Appl. Catal. B: Environ. 75 (2007) 78–87.
[41] J. Theis, H.-W. Jen, R. McCabe, M. Sharma, V. Balakotaiah, M.P. Harold, Soc. Automot. Eng. Tec., 2006-01-1067 (2006) http://dx.doi.org/10.4271/2006-01-1067
[42] C. Sedlmair, K. Seshan, A. Jentys, J.A. Lercher, J. Catal. 214 (2003) 308–316.
[43] B. Westerberg, E. Fridell, J. Mol. Catal. A: Chem. 165 (2001) 249–263.
[44] W.S. Kijlstra, D.S. Brands, E.K. Poels, A. Bliek, J. Catal. 171 (1997) 208–218.
[45] W.S. Kijlstra, D.S. Brands, H.I. Smit, E.K. Poels, A. Bliek, J. Catal. 171 (1997) 219–230.
[46] G. Centi, S. Perathoner, D. Biglino, E. Giamello, J. Catal. 152 (1995) 75–92.
[47] J.A. Anderson, G.J. Millar, C.H. Rochester, J. Chem. Soc. Faraday Trans. 86 (1990) 571–576.
[48] L. Lietti, I. Nova, P. Forzatti, J. Catal. 257 (2008) 270–282.
[49] J. Szanyi, J.H. Kwak, R.J. Chimentao, C.H.F. Peden, J. Phys. Chem. C 111 (2007) 2661–2669.
[50] R.L. Muncrief, P. Khanna, K.S. Kabin, M.P. Harold, Catal, Today 98 (2004) 393–402.
[51] B.-B. Chen, C. Shi, M. Crocker, Y. Wang, A.-M. Zhu, Appl. Catal. B: Environ. 132–133 (2013) 245–255.
[52] Y. Su, K.S. Kabin, M.P. Harold, M.D. Amiridis, Appl. Catal. B: Environ. 71 (2007) 207–215.
[53] Y.J. Ren, M.P. Harold, ACS Catal. 1 (2011) 969–988.
[54] W.S. Epling, C.H.F. Peden, J. Szanyi, J. Phys. Chem. C 112 (2008) 10952–10959.
[55] J. Pihl, J. Parks, C. Daw, T. Root, Soc. Automot. Eng. Tec., 2006-01-3441 (2006) http://dx.doi.org/10.4271/2006-01-3441